galaxies

MDPI

Article

Spectral Line VLBI Studies Using the ngEHT

Dong-Jin Kim [1,2,*,†] and Vincent Fish [1,†]

[1] Massachusetts Institute of Technology Haystack Observatory, Westford, MA 01886, USA
[2] Max-Planck-Institut für Radioastronomie, Auf dem Hügel 69, 53121 Bonn, Germany
* Correspondence: dongjink@mit.edu
† These authors contributed equally to this work.

Abstract: Spectroscopy in the mm/sub-mm wavelength range is a powerful tool to study the gaseous medium in various astrophysical environments. The next generation Event Horizon Telescope (ngEHT) equipped with a wide-bandwidth backend system has great potential for science using high angular resolution spectroscopy. Spectral line VLBI studies using the ngEHT will enable us to scrutinize compact astrophysical objects obscured by an optically thick medium on unprecedented angular scales. However, the capabilities of ngEHT for spectroscopy and specific scientific applications have not been properly envisioned. In this white paper, we briefly address science cases newly achievable via spectral line VLBI observations in the mm/sub-mm wavelength ranges, and suggest technical requirements to facilitate spectral line VLBI studies in the ngEHT era.

Keywords: very long baseline interferometry (1769); radio astronomy (1338); millimeter astronomy (1061); submillimeter astronomy (1647); radio telescopes (1360); high angular resolution (2167)

Citation: Kim, D.-J.; Fish, V. Spectral Line VLBI Studies Using the ngEHT. *Galaxies* **2023**, *11*, 10. https://doi.org/10.3390/galaxies11010010

Academic Editor: Luigina Feretti

Received: 18 November 2022
Revised: 30 December 2022
Accepted: 1 January 2023
Published: 6 January 2023

1. Introduction

The next generation Event Horizon Telescope (ngEHT) is primarily designed to image the continuum emission from the vicinity of the photon ring of supermassive black holes (SMBHs) with a better imaging performance than that of the current EHT array in terms of sensitivity and sampling in the spatial-frequency domain. A major upgrade of the ngEHT would be a new front and back end system, supporting a bandwidth of 8 GHz per sideband, dual polarization, and simultaneous dual band 230/345 GHz capability with a recording rate of 256 Gbps [1]. This new capability provokes interest for spectral line studies using the ngEHT for two reasons: (1) VLBI observations with such a wide bandwidth enable spectral line studies without additional frequency tunings at each station, and (2) the ngEHT offers several orders of magnitude higher angular resolutions than those available with single-dish telescopes or connected arrays, such as SMA, NOEMA, and ALMA. Microarcsecond scale angular resolution in spectral line studies would open new doorways to explore intriguing physical phenomena in compact astrophysical systems, such as the core of star-forming regions (SFRs), circumstellar envelope (CSE) of evolved stars, and circumnuclear disk (CND) of active galactic nuclei (AGNs).

Spectral line studies with a mm/sub-mm VLBI array and their possible scientific impacts have attracted the attention of researchers in recent years, especially due to the significant increase in sensitivity provided by the Atacama Large Millimeter/submillimeter Array (ALMA) Phasing System [2–5]. ALMA has already offered a prototype spectral line VLBI capability in Band 3 (3.5 mm) in conjunction with the Global mm-VLBI Array (GMVA) and anticipates offering more flexible spectral line VLBI modes in additional bands in the near future. However, much work is still needed to utilize its unique capability for VLBI studies. One of the most pressing tasks is to categorize possible candidates and types of spectral lines suited for mm/sub-mm VLBI experiments. In this context, here we highlight the types of spectral line sources available for VLBI studies and their potential use in various scientific applications.

2. Molecular Maser Lines

Microwave amplification by stimulated emission of radiation (maser) is a non-thermal process in the interstellar medium (ISM) that can result in remarkably bright spectral line emission. Molecular maser lines were discovered in both galactic and extragalactic sources [6–8]. The physical sizes of masing clouds measured by interferometric observations range from sub-AU to a few AU for galactic masers and sub-pc to pc scales for extragalactic masers [9,10]. Considering the distance and physical size of maser sources, their angular scale is typically a milli-arcsecond (mas). For instance, a galactic maser source with a physical scale of 1 AU corresponds to an angular scale of 1 mas at a source distance of ∼1000 pc. In this case, a proper motion of 10 km s^{-1} (∼2.1 AU yr^{-1}) corresponds to 2.1 mas yr^{-1} with an additional annual parallax of up to 1 mas. Monitoring VLBI observations at cm/mm wavelengths over a few months allow us to measure the proper motion or annual parallax of nearby galactic maser sources. VLBI observations at shorter wavelengths (mm/sub-mm) achieve higher angular resolutions, which can enlarge the number of spectral line source for astrometry, such as more distant galactic maser sources (>a few kpc) or sporadic maser features that last only a few weeks or less. In addition, mm/sub-mm maser transitions are theorized to have distinct excitation conditions, and hence they can unveil different part of the gaseous medium that cannot be traced by conventional maser transitions available at cm wavelengths [11,12].

2.1. Circumstellar Envelope of AGB Stars

In the late stages of stellar evolution, the outer layers of intermediate mass stars (1–8 $M_\odot$) expand to a few AU in radius, pulsating with a period of up to several years [13]. They are called asymptotic giant branch (AGB) stars, and their strong stellar winds (10–30 km s^{-1}) form a thick circumstellar envelope (CSE) [14]. AGB stars show morphological transitions of CSEs on relatively short time scales (10^5–10^6 yr), evolving into planetary nebulae (PNs) [14]. Despite such drastic changes, CSEs are known as the cradle of complex molecular species owing to their dense and cool environments, which are well-suited for molecular synthesis [15]. The characteristics of CSEs vary depending on their chemical and physical environments. For instance, the chemical composition of AGB stars determines the strength of stellar winds driven by heated dust [16]. Meanwhile, the presence of a companion star or giant planet likely plays an important role in the morphological evolution of CSEs, such as spiral patterns, collimated jets, and multi-polar structures [17,18]. To investigate the evolution of CSEs, multiple different types of AGB stars need to be studied separately, tracing stellar winds from the inner to the outer part of the CSEs.

In oxygen-rich (O-rich) AGB stars, SiO masers show a symmetric ring-like structure within a few stellar radii (R_*), while H_2O masers are located farther out up to a few tens of stellar radii with either symmetric or asymmetric spatial distributions [19–21]. To understand the development of asymmetric structure, it is necessary to probe the region between symmetric SiO masers and asymmetric H_2O masers clouds. According to radiative transfer models, the sub-mm H_2O maser emission at 321 GHz traces denser and warmer regions (2–5 R_*) compared to physical conditions required for masing at 22 GHz (2–10 R_*) [11,22]. VLBI observations of 321 GHz H_2O masers using the 345 GHz ngEHT receivers can test this theoretical prediction, constraining the size of masing clouds down to sub-AU scales (e.g., 15 µas ∼ 0.015 AU at 1 kpc distance) and also fill in the gap in our understanding of the development of stellar winds in CSEs. In contrast, carbon-rich (C-rich) AGB stars mainly form carbon-based molecules in their CSEs, and thus maser lines from oxygen-bearing molecules (e.g., H_2O, SiO, and OH) are barely detected in their CSEs. Spectral line surveys have detected HCN and SiS maser lines in the sub-mm wavelength range, and these lines seem widespread in C-rich AGB stars [23,24]. The CSEs of C-rich AGB stars are supposed to generate stronger stellar winds than those in O-rich AGB stars, but much is unknown about their kinematics due to the lack of high-resolution observations [16]. VLBI observations of HCN masers in C-rich AGB stars would shed light on this matter by spatially resolving maser spots and measuring their proper motions.

2.2. Star-Forming Regions

Gravitational collapse of clouds in the ISM triggered by internal or external physical conditions forms dense and compact clumps suited for star formation. Since star-forming regions (SFRs) are optically thick, much is still unknown about the process of star formation and differences in regions of high- and low-mass star formation [25] (and references therein). A variety of maser lines observed in massive SFRs (e.g., OH, H_2O, class I and II CH_3OH masers) are unique tools to classify different stages or classes of star formation. For instance, two distinct types of methanol masers excited collisionally (class I) or radiatively (class II) trace outer and inner regions of SFRs, respectively [26,27]. VLBI observations of class II methanol masers have shown complex inner structure in SFRs, including a ring-like structure [28–30]. On the contrary, class I methanol masers have revealed outflow features at a large distance from the central object [31]. Proper motion measurements via multi-epoch VLBI campaigns show diverse kinematics within scales of a few hundred AU, such as infall, outflow, and rotation. On the other hand, maser lines are rarely detected in low- and intermediate-mass SFRs compared to those in high-mass SFRs [32,33]. H_2O and methanol masers detected in some low-mass SFRs likely trace the inner parts of outflows [34]. Observations in the sub-mm wavelength range have detected new types of H_2O and CH_3OH maser lines in SFRs, but they have not been spatially resolved due to insufficient angular resolutions. [35–38]. Their excitation conditions are different from those of cm maser lines, suggesting the possibility to probe different parts of SFRs via VLBI observations [27]. Kinematics of clumpy molecular clouds revealed by VLBI observations will advance our understanding on the process of star-formations.

2.3. Circumnuclear Gas of AGNs

Extraordinarily bright maser lines (e.g., H_2O and OH) have been detected in a number of active galactic nuclei (AGNs) at cm wavelengths. VLBI observations show that they originate in either the accretion disk or outflow in the circumnuclear region of AGNs [10]. Measurements of the angular scale and rotational curve of the disk masers in AGNs provide an accurate measurement of the mass of the SMBHs [39,40]. The host galaxies of H_2O megamaser sources are commonly Seyfert galaxies, having relatively small SMBH masses (10^6–10^8 $M_\odot$) [41]. H_2O masers are very rare in elliptical galaxies. NGC 1052 and NGC 4261 are two such cases where the line profiles and VLBI observations indicate that the 22 GHz H_2O masers are likely associated with the ambient ISM interacting with radio jets [42,43]. Sub-mm H_2O masers have been detected in a number of AGNs, but their fine structure has not been spatially resolved [44–46]. VLBI observations of those sub-mm masers have potential to explore nuclear region of AGNs, such as molecular outflows, inner structure of molecular accretion disks, or jet-ISM interactions. We note that VLBI observations of 22 GHz H_2O masers towards the nearby AGN NGC 3079 show clumpy clouds with size in the range of 0.002 to 0.02 pc [9]. The ngEHT observations at 345 GHz offer an angular resolution of ∼15 µas (15 µas = ∼0.0015 pc at 20 Mpc distance), which can resolve a compact circumnuclear gas cloud in a nearby AGN.

3. Atomic Maser Lines

Ionized H II regions are known as the site of radio recombination lines (RRLs). In ionized regions, hydrogen RRLs sometimes show maser features in the sub-mm wavelength range [47]. Thanks to their high brightness temperatures, atomic maser lines are promising candidates for spectral line VLBI observations. The ionized region is commonly identified by optical emission lines (e.g., Hα), but a thick ambient medium often absorbs or reflects the optical emission from the ionized H II regions. Atomic maser lines in the radio wavelength range are optically thin, and thus help scrutinize gas kinematics in the obscured ionized region.

3.1. Post-AGB Stars and Pre-Planetary Nebulae

At the end of the AGB phase, the central star starts to ionize its surrounding materials. The ionized core region is the key to understand the development of asymmetric multi-polar jets or winds seen in PNs, but a dense dusty envelope heavily obscures the central region, impeding investigations of the core region of CSEs during the post-AGB and pre-planetary nebulae (pPNe) phases. η Carinae is the first RRL maser source detected in AGB stars [48]. ALMA observations of H30α emission show that a slightly blueshifted narrow line feature in the H30α spectrum is extended, but broad line features are compact [49,50]. More RRL maser sources have been detected in post-AGB stars, and they are characterized by different line profiles [51]. Follow-up high-resolution observations towards those RRL masers are necessary to clarify their origins and possible connections with bipolar/multi-polar outflows in the early phase of post-AGB stars.

3.2. Ultra-Compact H II Regions of Massive Stars

Strong radiation from newborn massive stars forms ionized regions. In the process of massive star formation, the ambient medium is thick and dense enough to cover the ionized region. This type of object is known as an ultra-compact (UC) H II region. Unveiling the kinematics of UC H II region is one of the most important topics in the study of star-formation. Theoretical studies point out that feedback from young stars prevents further matter accretion in high-mass star formations. However, somehow high-mass stars do exist in various star-forming regions. Studying hyper-compact (HC) H II regions might hint how matter keeps accreting during the early stage of high-mass star formation [52,53].

RRLs appear in ionized gas, such as UC H II regions. Since ionized gas also radiates continuum emission, line/continuum ratio is an important parameter to detect RRL. At sub-mm wavelengths, the line/continuum ratio increases remarkably and maser emission can arise in certain local conditions. MWC 349 is the high-mass star-forming region, showing RLL maser at sub-mm wavelengths [54]. The H30α maser emission in MWC 349 traces the innermost regions of the cocoon. Submillimeter Array (SMA) observations of RRL maser reveal an ionized accretion disk in MWC 349 [55]. More RRL masers sources have been detected in UC H II region. The double-peaked RRL maser spectrum with very broad line widths (up to a few hundreds km s^{-1}) suggests that RRL masers are associated with a bi-conical or collimated radio jet [56,57]. High-angular resolution VLBI observations towards RRL maser lines are needed to unveil the nuclear region of very young massive stars.

4. Molecular Absorption Lines

Molecular clouds become visible in absorption against the featureless continuum emission of the AGN jet. Absorption studies allow us to detect even low abundance molecular species regardless of their cosmological distance if the continuum jet is bright enough, effectively using the jet as a strong flashlight to illuminate the material. The absorption technique can be used to access any intervening molecular clouds lying on the line of sight. Spectral-line VLBI observations towards molecular absorption lines spatially resolve the structure and kinematics of the obscuring molecular clouds, and therefore can clarify the origin of obscuring molecular clouds. Gravitationally lensed blazars (GLB) and circumnuclear gas in radio AGNs are well-known such systems, showing molecular absorption lines from the intervening molecular clouds. Previous absorption studies focused on cm wavelengths hint interaction between radio jets and ambient medium [58,59], but observable molecular species and angular resolutions are limited. In the sub-mm range, various molecular species in different chemical environments are detectable in absorption with improved angular resolutions. Therefore, mm/sub-mm absorption line studies are desirable to advance our understanding on the chemistry of extragalactic ISM and kinematics of circumnuclear molecular gas in radio AGNs.

4.1. Gravitationally Lensed Blazars

PKS 1830-211 is one of the most well-known gravitationally lensed blazar systems, consisting of a distant blazar at a redshift of 2.5 and a face-on spiral galaxy at a redshift of 0.89 [60]. The blazar serves as a background continuum source for the intervening galaxy, and thus various molecular lines have been detected in absorption. With bright continuum, absorption line observations allow us to detect rare molecular species compared to observations using emission lines. Indeed, over 50 molecular species have been detected in the intervening spiral galaxy via absorption lines [60–64]. However, observations using single-dish telescopes or connected arrays tend to underestimate absorption depths due to low filling factors, since the beam size is larger than the size of absorbed area [65]. Absorption line observations using VLBI can spatially resolve individual continuum components related to absorption features, hence providing a better physical constraint on the obscuring molecular gas. Furthermore, VLBI monitoring of molecular absorption lines can provide a unique tool to study a structural variation of the background blazar through absorption line variability at multiple frequency bands [66].

4.2. Circumnuclear Gas in AGNs

AGNs are among the most powerful energy sources in the Universe. The radio jet outflows triggered by AGN activity are believed to play an important role in galaxy formation and evolution [67–69]. However, the nature of different types of radio jets and their influence on their host galaxies (i.e., radio jet feedback) are still poorly understood. As a matter reservoir in the vicinity of the central engine, the circumnuclear gas is the key to study different accretion environments and radio jet feedback in AGNs harboring radio jets (i.e., radio AGNs). Although radio AGNs tend to be gas-poor and distant, molecular absorption line observations using bright continuum radio jets enable us to study the circumnuclear gas. Sparse molecular species can be detected in absorption, providing a unique tool to study the small-scale (<pc) structure of the circumnuclear gas via spectral-line VLBI observations. Such high resolution observations are particularly important to reveal the onset of radio jet feedback or the fate of a fueling flow in the vicinity of the central engine. Despite the advantages of absorption line study, only a handful of radio AGNs have been identified as molecular absorption systems. In the sub-mm wavelength range, plenty of molecular lines are available for absorption line observations. Indeed, recent ALMA observations shows molecular absorption lines in radio AGNs [70–72]. VLBI observations towards sub-mm molecular absorption lines are the next step to clarify the origin of obscuring gas in radio AGNs and their roles in AGN fueling and feedback.

5. Technical Overview for Spectroscopy

5.1. Spectral Line Sensitivity

New ngEHT stations may have an aperture size of 10 m or less, resulting in a lower spectral line sensitivity on new baselines than for the current EHT array. Assuming a conventional quantization loss in the data recording process (η_s = 0.8), the expected spectral line sensitivities of ngEHT$_{6\,m}$-ALMA and ngEHT$_{6\,m}$-ngEHT$_{6\,m}$ baselines are 88 mJy and 1040 mJy, respectively with an integration time of 15 min and a spectral resolution of 1 MHz at 345 GHz (see Table 1). An order of magnitude higher spectral line sensitivity can be achievable by adding ALMA as an anchor station. Therefore, the optimal configuration of the ngEHT for spectral line VLBI observations would be including NOEMA and ALMA as anchor stations. This will provide exquisite spectral line sensitivity for sources in both the northern and southern hemispheres. Despite its relatively small aperture size, additional ngEHT stations will eventually improve the total spectral line sensitivity of ngEHT array by increasing the number of baselines ($N_{baseline} = N_{ant}(N_{ant}-1)/2$). Considering the expected spectral line sensitivity, a minimum peak flux density of a narrow maser emission line (FWHM $< 10\,\mathrm{km\,s^{-1}}$) would be >10 Jy and >20 Jy at 230 GHz and 345 GHz, respectively for imaging the spectral line with the standalone ngEHT array. Table 2 shows a representative sub-mm spectral line sources mentioned in Sections 2–4 with line parameters.

Table 1. Single-dish spectral line sensitivity of ngEHT stations with an integration time of 15 min at 230 GHz and 345 GHz, respectively.

Antenna	Aperture Size	1 σ at 230 GHz 1 MHz (1.3 km s^{-1})	1 σ at 345 GHz 1 MHz (0.8 km s^{-1})
ngEHT-Small	6 m	474 mJy	832 mJy
ngEHT-Large	10 m	282 mJy	496 mJy
NOEMA	15 m × 12 ∼ 26 m	9.6 mJy	15 mJy
ALMA	12 m × 50 ∼ 42 m	2.8 mJy	6 mJy

Note: Aperture efficiencies are 0.8, 0.67, 0.8 at 230 GHz and 0.8, 0.62, 0.7 at 345 GHz for ngEHT, NOEMA, and ALMA stations, respectively. The same amount of precipitable water vapor (PWV) was assumed at all stations (3 mm at 230 GHz and 1 mm at 345 GHz). Reference: https://www.iram.fr/GENERAL/NOEMA-Phase-A.pdf. Accessed on 30 December 2022.

Table 2. Different types of spectral line sources at sub-mm wavelengths.

Type	Name	Source	Transition	Peak Flux (Jy beam^{-1})	Line Width (km s^{-1})	Beam Size (arcsec × arcsec)
Molecular maser	VY Cma [a]	AGB	H_2O 10_{29}–9_{36}	500	< 10	0.75 × 0.75
	G358.93-0.03 [b]	SFR	CH_3OH 13_{-1}–14_{-2}	270	< 5	0.46 × 0.42
	Circinus [c]	AGN	H_2O 10_{29}–9_{36}	1.5	< 10	0.33 × 0.21
Atomic maser	η Carinae (core) [d]	post-AGB	H30α	5.5	28	0.09 × 0.09
	MWC 349 [e]	SFR	H30α	24–40	4–5	1.20 × 0.90
				Cont/Line (mJy beam^{-1})	Line width (km s^{-1})	Beam size (arcsec × arcsec)
Molecular absorption	PKS 1830-211 [f]	GLB	H_2O 1_{10}–1_{01}	700/210 (NE) 570/541 (SW)	< 53 53	0.50 × 0.50
	NGC 1052 [g]	AGN	CO J=3–2	442/37	169	0.21 × 0.21

Reference: [a] [73–75]. [b] [76] [c] [46]. [d] [49,50]. [e] [54,55]. [f] [77] [g] [71].

Adding an anchor station, such as ALMA and NOEMA will lower those limits by a factor of 12. Observations of a broad (FWHM > 10 km s^{-1}) absorption or emission line with a moderate spectral resolution will enlarge the number of detectable spectral line sources with the ngEHT. In previous H_2O maser surveys in the cm/mm wavelength ranges, about 2300 H_2O maser sources have been detected (SFR: ∼1400, AGB: ∼700, and extragalactic: ∼180) [38,78]. Assuming 5% detection rate of bright (>20 Jy) sub-mm H_2O maser among known maser sources, about 115 sources will be feasible targets for the ngEHT. Observations of other sub-mm maser species, such as CH_3OH and SiO, will increase the number of available targets to a few hundreds. Meanwhile, an increased coherence time by frequency phase transfer (FPT) technique will further improve the spectral line sensitivity of ngEHT [79,80], but a detailed investigation is needed to evaluate the capability of FPT for spectral line VLBI observations.

5.2. Frequency Coverage

A simultaneous triple-band (3 mm, 1 mm, and 0.8 mm) receiver system has been considered for the ngEHT to apply the FPT technique. Simultaneous multi-band VLBI observations can yield several atomic and molecular lines in a single run. This unique capability is beneficial for spectral line VLBI studies in various aspects. For instance, a combined study using multiple VLBI images of different molecular maser lines would provide a comprehensive view of a masing region [21,81]. In case of molecular absorption line studies, observing multiple rotational lines provides solid constraints on the physical quantities of the obscuring gas, such as temperature and column density. We note that the observing frequency of 1 mm and 0.8 mm receivers should have integer frequency ratios of the 3 mm receiver for FPT. This technical requirement would help simultaneous observations of several rotational lines at different bands, such as HCN, HCO+, SiO, and CO. However, simultaneous multi-band observations will result in narrower bandwidth at each band than single-band observations due to a limited recording rate of the backend system. Therefore, we need to consider several spectral line observation modes for individual science projects. For instance, non-integer and wide bandwidth observations are preferred

for RRL maser line observations. On the contrary, integer and multi-band observations are preferred for molecular maser or absorption line observations. In practice, offering a flexible frequency setup would not be feasible in the early phase of array operation. Therefore, we suggest two optimal frequency tunings for 8 GHz and 16 GHz bandwidth observations, respectively considering continuum observations with FPT. Specific frequency tunings and distribution of spectral lines are present in Table 3 and Figure 1.

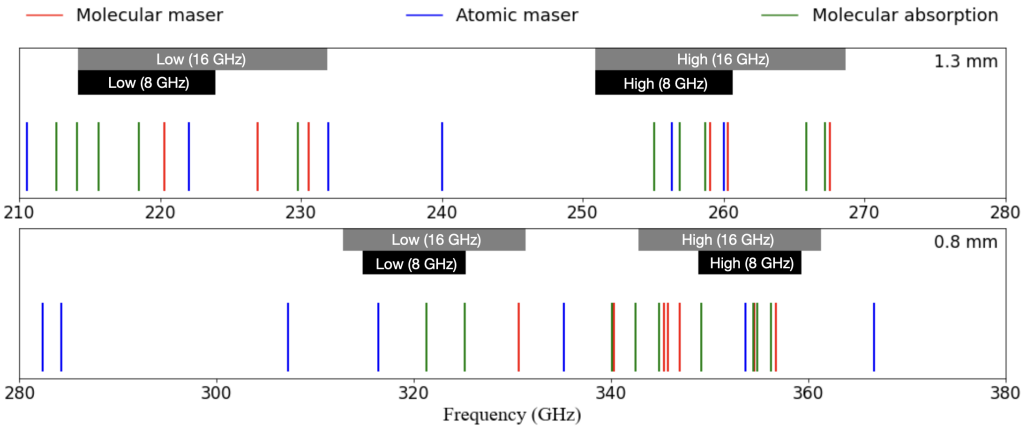

Figure 1. Distribution of spectral lines over the frequency range of 1.3 mm and 0.8 mm. Each color indicates the type of spectral lines. Frequency coverage of 8 GHz and 16 GHz observations is marked with two different frequency tunings (low and high).

Table 3. Suggested frequency tunings with different bandwidths (8 GHz and 16 GHz) at each band for spectral line VLBI observations.

Frequency (GHz)	Bandwidth (GHz)	Frequency (GHz)	Primary Target
230_{low}	8	215–223	SiO, CH_3OH, Hβ
230_{high}	8	252–260	SiO, Hα
345_{low}	8	316–324	H_2O, Hα
345_{high}	8	350–358	HCN, HCO+, Hα, H_2O
230_{low}	16	215–231	CO, SiO, CH_3OH, CN Hβ
230_{high}	16	252–268	SiO, Hα, HCN, HCO+
345_{low}	16	314–330	H_2O Hα
345_{high}	16	344–360	CO, HCN, HCO+, Hα, H_2O, SiO

6. Conclusions

The ngEHT will be equipped with multi-band receivers supporting simultaneous wideband observations. It will not only improve sensitivity for continuum imaging, but also open new opportunities for high angular resolution spectroscopy. In this white paper, we have outlined the types of spectral lines suited for VLBI studies and briefly described several scientific applications newly achievable with the ngEHT. Spectral lines observable with the 230 and 345 GHz receivers are listed in Table 4. Masers appear in various astrophysical environments, and they trace certain chemical and physical environments depending on atomic/molecular species and transitions. Atomic and molecular maser lines observable in the sub-mm wavelength range possibly unveil regions unprobed by previous cm-maser observations. The ngEHT can be used to image sub-mm masers, investigating their peculiar physical environments and kinematics.

Table 4. Selected spectral lines near 230 GHz and 345 GHz and their energy level above ground state. Three different types of spectral lines available for VLBI observations are listed with physical origins.

Type	Frequency (GHz)	Transition	E_{low} (K)	Source
Molecular masers	214.088	^{28}SiO v = 2, J=5–4	3541	O-rich AGB
	215.596	^{28}SiO v = 1, J=5–4	1790	O-rich AGB
	256.898	^{28}SiO v = 2, J=6–5	3551	O-rich AGB
	258.707	^{28}SiO v = 1, J=6-5	1800	O-rich AGB
	299.704	^{28}SiO v = 2, J=7–6	3564	O-rich AGB
	301.814	^{28}SiO v = 1, J=7–6	1813	O-rich AGB
	342.504	^{28}SiO v = 2, J=8–7	3579	O-rich AGB
	344.916	^{28}SiO v = 1, J=8–7	1827	O-rich AGB
	265.853	HCN (0, 1^{1e}, 0), J=3–2	1050	C-rich AGB
	267.199	HCN (0, 1^{1f}, 0), J=3–2	1050	C-rich AGB
	354.460	HCN (0, 1^{1e}, 0), J=4–3	1067	C-rich AGB
	356.256	HCN (0, 1^{1f}, 0), J=4–3	1067	C-rich AGB
	218.440	CH_3OH 4_2–3_1	24	SFRs (class I)
	229.759	CH_3OH 8_{-1}–7_0	54	SFRs (class I)
	343.599	CH_3OH 13_{-1}–14_{-2}	607	SFRs (class II)
	349.107	CH_3OH 14_1–14_0	243	SFRs (class II)
	321.226	H_2O 10_{29}–9_{36}	1846	SFRs/AGB/AGNs
	325.153	H_2O 5_{14}–4_{22}	454	SFRs/AGB/AGNs
	354.809	H_2O $17_{4,13}$–$4_{7,10}$	5764	SFRs/AGB/AGNs
Atomic masers	210.502	H31α		SFRs
	231.900	H30α		SFRs
	256.302	H29α		SFRs
	284.251	H28α		SFRs
	316.415	H27α		SFRs
	353.623	H26α		SFRs
	222.012	H38β		SFRs
	240.021	H37β		SFRs
	260.033	H36β		SFRs
	282.333	H35β		SFRs
	307.258	H34β		SFRs
	335.207	H33β		SFRs
	366.653	H32β		SFRs
Molecular absorption	220.299	^{13}CO J=2–1	5	AGNs/GLB
	230.538	CO J=2–1	6	AGNs/GLB
	330.588	^{13}CO J= 3–2	16	AGNs/GLB
	345.796	CO J=3–2	17	AGNs/GLB
	265.886	HCN J=3–2	13	AGNs/GLB
	354.505	HCN J=4–3	26	AGNs/GLB
	267.558	HCO+ J=3–2	13	AGNs/GLB
	356.734	HCO+ J=4–3	18	AGNs/GLB
	259.012	H^{13}CN J=3–2	9	AGNs/GLB
	345.340	H^{13}CN J=4–3	17	AGNs/GLB
	260.255	H^{13}CO+ J=3–2	9	AGNs/GLB
	346.998	H^{13}CO+ J=4–3	18	AGNs/GLB
	226.874	CN N=2–1, J=5/2–3/2	5	AGNs/GLB
	340.247	CN N=3–2, J=7/2–5/2	16	AGNs/GLB

Note: Rest frequencies were obtained from the Splatalogue database available at www.splatalogue.net. Accessed on 30 December 2022.

However, VLBI experiments with maser lines could be challenging due to the limited spectral line sensitivity of the ngEHT and the rarity of sub-mm masers compared to cm/mm masers. Absorption line observations using a bright background continuum source (e.g., radio jet) are an alternative approach to enable spectral line VLBI studies towards common molecular clouds regardless of their distance. Molecular absorption from circumnuclear gas in AGNs or the intervening galaxy of a lensed blazar are promising candidates for spectral

line VLBI studies. Lastly, we have highlighted the capabilities of ngEHT for spectroscopy. Considering the rest frequencies of atomic and molecular transitions, we suggest frequency tunings to facilitate the operation of ngEHT in spectral line mode.

Author Contributions: Conceptualization, D.-J.K.; methodology, D.-J.K.; writing—original draft, D.-J.K.; writing—review and editing, V.F.; supervision, V.F. All authors have read and agreed to the published version of the manuscript.

Funding: This research was supported by the National Science Foundation through grant numbers AST-1935980 and AST-2034306.

Data Availability Statement: Not applicable.

Conflicts of Interest: The authors declare no conflict of interest.

References

1. Doeleman, S.; Blackburn, L.; Dexter, J.; Gomez, J.L.; Johnson, M.D.; Palumbo, D.C.; Weintroub, J.; Farah, J.R.; Fish, V.; Loinard, L.; et al. Studying Black Holes on Horizon Scales with VLBI Ground Arrays. *Proc. Bull. Am. Astron. Soc.* **2019**, *51*, 256.
2. Fish, V.; Alef, W.; Anderson, J.; Asada, K.; Baudry, A.; Broderick, A.; Carilli, C.; Colomer, F.; Conway, J.; Dexter, J.; et al. High-Angular-Resolution and High-Sensitivity Science Enabled by Beamformed ALMA. *arXiv* **2013**, arXiv:1309.3519.
3. Tilanus, R.P.J.; Krichbaum, T.P.; Zensus, J.A.; Baudry, A.; Bremer, M.; Falcke, H.; Giovannini, G.; Laing, R.; van Langevelde, H.J.; Vlemmings, W.; et al. Future mmVLBI Research with ALMA: A European vision. *arXiv* **2014**, arXiv:1406.4650.
4. Asada, K.; Kino, M.; Honma, M.; Hirota, T.; Lu, R.S.; Inoue, M.; Sohn, B.W.; Shen, Z.Q.; Ho, P.T.P.; Akiyama, K.; et al. White Paper on East Asian Vision for mm/submm VLBI: Toward Black Hole Astrophysics down to Angular Resolution of 1~R $_S$. *arXiv* **2017**, arXiv:1705.04776.
5. Matthews, L.D.; Crew, G.B.; Doeleman, S.S.; Lacasse, R.; Saez, A.F.; Alef, W.; Akiyama, K.; Amestica, R.; Anderson, J.M.; Barkats, D.A.; et al. The ALMA Phasing System: A Beamforming Capability for Ultra-high-resolution Science at (Sub)Millimeter Wavelengths. *Publ. Astron. Soc. Pac.* **2018**, *130*, 015002. [CrossRef]
6. Litvak, M.M. Coherent molecular radiation. *Annu. Rev. Astron. Astrophys.* **1974**, *12*, 97–112. [CrossRef]
7. Reid, M.J.; Moran, J.M. Masers. *Annu. Rev. Astron. Astrophys.* **1981**, *19*, 231–276. [CrossRef]
8. Elitzur, M. Astronomical masers. *Annu. Rev. Astron. Astrophys.* **1992**, *30*, 75–112. [CrossRef]
9. Trotter, A.S.; Greenhill, L.J.; Moran, J.M.; Reid, M.J.; Irwin, J.A.; Lo, K.Y. Water Maser Emission and the Parsec-Scale Jet in NGC 3079. *Astrophys. J.* **1998**, *495*, 740–748. [CrossRef]
10. Lo, K.Y. Mega-Masers and Galaxies. *Annu. Rev. Astron. Astrophys.* **2005**, *43*, 625–676. [CrossRef]
11. Gray, M.D.; Baudry, A.; Richards, A.M.S.; Humphreys, E.M.L.; Sobolev, A.M.; Yates, J.A. The physics of water masers observable with ALMA and SOFIA: Model predictions for evolved stars. *Mon. Not. R. Astron. Soc.* **2016**, *456*, 374–404. [CrossRef]
12. Bergman, P.; Humphreys, E.M.L. Submillimetre water masers at 437, 439, 471, and 474 GHz towards evolved stars. APEX observations and radiative transfer modelling. *Astron. Astrophys.* **2020**, *638*, A19. [CrossRef]
13. Herwig, F. Evolution of Asymptotic Giant Branch Stars. *Annu. Rev. Astron. Astrophys.* **2005**, *43*, 435–479. [CrossRef]
14. Höfner, S.; Olofsson, H. Mass loss of stars on the asymptotic giant branch. Mechanisms, models and measurements. *Astron. Astrophys. Rev.* **2018**, *26*, 1. [CrossRef]
15. Gail, H.P.; Sedlmayr, E. *Physics and Chemistry of Circumstellar Dust Shells*; Cambridge University Press: Cambridge, UK, 2013, ISBN 978-0-5119-8560-7.
16. Woitke, P. Too little radiation pressure on dust in the winds of oxygen-rich AGB stars. *Astron. Astrophys.* **2006**, *460*, L9–L12. [CrossRef]
17. Huang, P.S.; Lee, C.F.; Sahai, R. Evolution from Spherical AGB Wind to Multipolar Outflow in Pre-planetary Nebula IRAS 17150-3224. *Astrophys. J.* **2020**, *889*, 85. [CrossRef]
18. Randall, S.K.; Trejo, A.; Humphreys, E.M.L.; Kim, H.; Wittkowski, M.; Boboltz, D.; Ramstedt, S. Discovery of a complex spiral-shell structure around the oxygen-rich AGB star GX Monocerotis. *Astron. Astrophys.* **2020**, *636*, A123. [CrossRef]
19. Diamond, P.J.; Kemball, A.J.; Junor, W.; Zensus, A.; Benson, J.; Dhawan, V. Observation of a Ring Structure in SiO Maser Emission from Late-Type Stars. *Astrophys. J. Lett.* **1994**, *430*, L61. [CrossRef]
20. Imai, H.; Shibata, K.M.; Marvel, K.B.; Diamond, P.J.; Sasao, T.; Miyoshi, M.; Inoue, M.; Migenes, V.; Murata, Y. The Three-dimensional Kinematics of Water Masers around the Semiregular Variable RT Virginis. *Astrophys. J.* **2003**, *590*, 460–472. [CrossRef]
21. Kim, D.J.; Cho, S.H.; Yun, Y.; Choi, Y.K.; Yoon, D.H.; Kim, J.; Dodson, R.; Rioja, M.J.; Yang, H.; Yoon, S.J. Simultaneous VLBI Astrometry of H_2O and SiO Masers toward the Semiregular Variable R Crateris. *Astrophys. J. Lett.* **2018**, *866*, L19. [CrossRef]
22. Humphreys, E.M.L.; Yates, J.A.; Gray, M.D.; Field, D.; Bowen, G.H. Qualitative reproduction of stellar H_2O maser morphology. I. Results at a single stellar phase. *Astron. Astrophys.* **2001**, *379*, 501–514. [CrossRef]
23. Gong, Y.; Henkel, C.; Ott, J.; Menten, K.M.; Morris, M.R.; Keller, D.; Claussen, M.J.; Grasshoff, M.; Mao, R.Q. SiS in the Circumstellar Envelope of IRC +10216: Maser and Quasi-thermal Emission. *Astrophys. J.* **2017**, *843*, 54. [CrossRef]

24. Menten, K.M.; Wyrowski, F.; Keller, D.; Kamiński, T. Widespread HCN maser emission in carbon-rich evolved stars. *Astron. Astrophys.* **2018**, *613*, A49. [CrossRef]
25. Evans, N.J., II. Physical Conditions in Regions of Star Formation. *Annu. Rev. Astron. Astrophys.* **1999**, *37*, 311–362. [CrossRef]
26. Cragg, D.M.; Johns, K.P.; Godfrey, P.D.; Brown, R.D. Pumping the interstellar methanol masers. *Mon. Not. R. Astron. Soc.* **1992**, *259*, 203–208. [CrossRef]
27. Cragg, D.M.; Sobolev, A.M.; Godfrey, P.D. Models of class II methanol masers based on improved molecular data. *Mon. Not. R. Astron. Soc.* **2005**, *360*, 533–545. [CrossRef]
28. Bartkiewicz, A.; Szymczak, M.; van Langevelde, H.J. Ring shaped 6.7 GHz methanol maser emission around a young high-mass star. *Astron. Astrophys.* **2005**, *442*, L61–L64. [CrossRef]
29. Bartkiewicz, A.; Szymczak, M.; van Langevelde, H.J.; Richards, A.M.S.; Pihlström, Y.M. The diversity of methanol maser morphologies from VLBI observations. *Astron. Astrophys.* **2009**, *502*, 155–173. [CrossRef]
30. Bartkiewicz, A.; Sanna, A.; Szymczak, M.; Moscadelli, L.; van Langevelde, H.J.; Wolak, P. The nature of the methanol maser ring G23.657-00.127. II. Expansion of the maser structure. *Astron. Astrophys.* **2020**, *637*, A15. [CrossRef]
31. Bartkiewicz, A.; van Langevelde, H.J. Masers in star forming regions. In Proceedings of the Cosmic Masers—From OH to H0, Stellenbosch, South Africa, 29 January–3 February 2012; Booth, R.S., Vlemmings, W.H.T., Humphreys, E.M.L., Eds.; Volume 287, pp. 117–126. [CrossRef]
32. Kalenskii, S.V.; Johansson, L.E.B.; Bergman, P.; Kurtz, S.; Hofner, P.; Walmsley, C.M.; Slysh, V.I. Search for Class I methanol masers in low-mass star formation regions. *Mon. Not. R. Astron. Soc.* **2010**, *405*, 613–620. [CrossRef]
33. Bae, J.H.; Kim, K.T.; Youn, S.Y.; Kim, W.J.; Byun, D.Y.; Kang, H.; Oh, C.S. A Multi-epoch, Simultaneous Water and Methanol Maser Survey toward Intermediate-mass Young Stellar Objects. *Astrophys. J. Suppl.* **2011**, *196*, 21. [CrossRef]
34. Moscadelli, L.; Testi, L.; Furuya, R.S.; Goddi, C.; Claussen, M.; Kitamura, Y.; Wootten, A. First results from a VLBA proper motion survey of H2O masers in low-mass YSOs: The Serpens core and RNO 15-FIR. *Astron. Astrophys.* **2006**, *446*, 985–999. [CrossRef]
35. Slysh, V.I.; Kalenskiĭ, S.V.; Val'tts, I.E. Methanol Radio Emission at Millimeter Wavelengths: New Masers at 1.3 and 2.8 Millimeters. *Astron. Rep.* **2002**, *46*, 49–56. [CrossRef]
36. van Kempen, T.A.; Wilner, D.; Gurwell, M. 183 GHz H_2O Maser Emission Around the Low-Mass Protostar Serpens SMM1. *Astrophys. J. Lett.* **2009**, *706*, L22–L26. [CrossRef]
37. Ladeyschikov, D.A.; Bayandina, O.S.; Sobolev, A.M. Online Database of Class I Methanol Masers. *Astron. J.* **2019**, *158*, 233. [CrossRef]
38. Ladeyschikov, D.A.; Sobolev, A.M.; Bayandina, O.S.; Shakhvorostova, N.N. Online Database of Multiwavelength Water Masers in Galactic Star-forming Regions. *Astron. J.* **2022**, *163*, 124. [CrossRef]
39. Kuo, C.Y.; Braatz, J.A.; Condon, J.J.; Impellizzeri, C.M.V.; Lo, K.Y.; Zaw, I.; Schenker, M.; Henkel, C.; Reid, M.J.; Greene, J.E. The Megamaser Cosmology Project. III. Accurate Masses of Seven Supermassive Black Holes in Active Galaxies with Circumnuclear Megamaser Disks. *Astrophys. J.* **2011**, *727*, 20. [CrossRef]
40. Pesce, D.W.; Braatz, J.A.; Condon, J.J.; Greene, J.E. Measuring Supermassive Black Hole Peculiar Motion Using H_2O Megamasers. *Astrophys. J.* **2018**, *863*, 149. [CrossRef]
41. Greene, J.E.; Seth, A.; Kim, M.; Läsker, R.; Goulding, A.; Gao, F.; Braatz, J.A.; Henkel, C.; Condon, J.; Lo, K.Y.; et al. Megamaser Disks Reveal a Broad Distribution of Black Hole Mass in Spiral Galaxies. *Astrophys. J. Lett.* **2016**, *826*, L32. [CrossRef]
42. Claussen, M.J.; Diamond, P.J.; Braatz, J.A.; Wilson, A.S.; Henkel, C. The Water Masers in the Elliptical Galaxy NGC 1052. *Astrophys. J. Lett.* **1998**, *500*, L129–L132. [CrossRef]
43. Wagner, J. 22 GHz water maser search in 37 nearby galaxies. Four new water megamasers in Seyfert 2 and OH maser/absorber galaxies. *Astron. Astrophys.* **2013**, *560*, A12. [CrossRef]
44. Humphreys, E.M.L.; Greenhill, L.J.; Reid, M.J.; Beuther, H.; Moran, J.M.; Gurwell, M.; Wilner, D.J.; Kondratko, P.T. First Detection of Millimeter/Submillimeter Extragalactic H_2O Maser Emission. *Astrophys. J. Lett.* **2005**, *634*, L133–L136. [CrossRef]
45. Humphreys, E.M.L. Submillimeter and millimeter masers. In Proceedings of the Astrophysical Masers and Their Environments, Alice Springs, Australia, 12–16 March 2007; Chapman, J.M., Baan, W.A., Eds.; Volume 242, pp. 471–480. [CrossRef]
46. Hagiwara, Y.; Horiuchi, S.; Imanishi, M.; Edwards, P.G. Second-epoch ALMA Observations of 321 GHz Water Maser Emission in NGC 4945 and the Circinus Galaxy. *Astrophys. J.* **2021**, *923*, 251. [CrossRef]
47. Gordon, M.A.; Sorochenko, R.L. *Radio Recombination Lines. Their Physics and Astronomical Applications*; Springer: Berlin/Heidelberg, Germany, 2002; Volume 282. [CrossRef]
48. Cox, P.; Martin-Pintado, J.; Bachiller, R.; Bronfman, L.; Cernicharo, J.; Nyman, L.A.; Roelfsema, P.R. Millimeter recombination lines toward η Carinae. *Astron. Astrophys.* **1995**, *295*, L39–L42.
49. Abraham, Z.; Falceta-Gonçalves, D.; Beaklini, P.P.B. η Carinae Baby Homunculus Uncovered by ALMA. *Astrophys. J.* **2014**, *791*, 95. [CrossRef]
50. Abraham, Z.; Beaklini, P.P.B.; Cox, P.; Falceta-Gonçalves, D.; Nyman, L.Å. η Carinae: High angular resolution continuum, H30α and He30α ALMA images. *Mon. Not. R. Astron. Soc.* **2020**, *499*, 2493–2512. [CrossRef]
51. Sánchez Contreras, C.; Báez-Rubio, A.; Alcolea, J.; Bujarrabal, V.; Martín-Pintado, J. A pilot search for mm-wavelength recombination lines from emerging ionized winds in pre-planetary nebulae candidates. *Astron. Astrophys.* **2017**, *603*, A67. [CrossRef]
52. Wolfire, M.G.; Cassinelli, J.P. Conditions for the Formation of Massive Stars. *Astrophys. J.* **1987**, *319*, 850. [CrossRef]

53. Cesaroni, R.; Galli, D.; Lodato, G.; Walmsley, M.; Zhang, Q. The critical role of disks in the formation of high-mass stars. *Nature* **2006**, *444*, 703–706. [CrossRef]
54. Martin-Pintado, J.; Thum, C.; Bachiller, R. Time-variable recombination line emission in MWC 349. *Astron. Astrophys.* **1989**, *222*, L9–L11.
55. Weintroub, J.; Moran, J.M.; Wilner, D.J.; Young, K.; Rao, R.; Shinnaga, H. Submillimeter Array Imaging of the Maser Emission from the H30α Radio Recombination Line in MWC 349A. *Astrophys. J.* **2008**, *677*, 1140–1150. [CrossRef]
56. Jiménez-Serra, I.; Martín-Pintado, J.; Báez-Rubio, A.; Patel, N.; Thum, C. Extremely Broad Radio Recombination Maser Lines Toward the High-velocity Ionized Jet in Cepheus A HW2. *Astrophys. J. Lett.* **2011**, *732*, L27. [CrossRef]
57. Jiménez-Serra, I.; Báez-Rubio, A.; Rivilla, V.M.; Martín-Pintado, J.; Zhang, Q.; Dierickx, M.; Patel, N. A New Radio Recombination Line Maser Object toward the MonR2 H II Region. *Astrophys. J. Lett.* **2013**, *764*, L4. [CrossRef]
58. Morganti, R.; Oosterloo, T.A.; Emonts, B.H.C.; van der Hulst, J.M.; Tadhunter, C.N. Fast Outflow of Neutral Hydrogen in the Radio Galaxy 3C 293. *Astrophys. J. Lett.* **2003**, *593*, L69–L72. [CrossRef]
59. Morganti, R.; Tadhunter, C.N.; Oosterloo, T.A. Fast neutral outflows in powerful radio galaxies: A major source of feedback in massive galaxies. *Astron. Astrophys.* **2005**, *444*, L9–L13. [CrossRef]
60. Wiklind, T.; Combes, F. The redshift of the gravitational lens of PKS1830-211 determined from molecular absorption lines. *Nature* **1996**, *379*, 139–141. [CrossRef]
61. Muller, S.; Guélin, M.; Dumke, M.; Lucas, R.; Combes, F. Probing isotopic ratios at z = 0.89: Molecular line absorption in front of the quasar PKS 1830-211. *Astron. Astrophys.* **2006**, *458*, 417–426. [CrossRef]
62. Muller, S.; Guélin, M. Drastic changes in the molecular absorption at redshift z = 0.89 toward the quasar PKS 1830-211. *Astron. Astrophys.* **2008**, *491*, 739–746. [CrossRef]
63. Henkel, C.; Braatz, J.A.; Menten, K.M.; Ott, J. The kinetic temperature of a molecular cloud at redshift 0.9: Ammonia in the gravitational lens PKS0-211. *Astron. Astrophys.* **2008**, *485*, 451–456. [CrossRef]
64. Menten, K.M.; Güsten, R.; Leurini, S.; Thorwirth, S.; Henkel, C.; Klein, B.; Carilli, C.L.; Reid, M.J. Submillimeter water and ammonia absorption by the peculiar z $\approx$ 0.89 interstellar medium in the gravitational lens of the PKS 1830-211 system. *Astron. Astrophys.* **2008**, *492*, 725–730. [CrossRef]
65. Muller, S.; Beelen, A.; Guélin, M.; Aalto, S.; Black, J.H.; Combes, F.; Curran, S.J.; Theule, P.; Longmore, S.N. Molecules at z = 0.89. A 4-mm-rest-frame absorption-line survey toward PKS 1830-211. *Astron. Astrophys.* **2011**, *535*, A103. [CrossRef]
66. Martí-Vidal, I.; Muller, S.; Combes, F.; Aalto, S.; Beelen, A.; Darling, J.; Guélin, M.; Henkel, C.; Horellou, C.; Marcaide, J.M.; et al. Probing the jet base of the blazar PKS 1830-211 from the chromatic variability of its lensed images. Serendipitous ALMA observations of a strong gamma-ray flare. *Astron. Astrophys.* **2013**, *558*, A123. [CrossRef]
67. Harrison, C.M.; Alexander, D.M.; Mullaney, J.R.; Swinbank, A.M. Kiloparsec-scale outflows are prevalent among luminous AGN: Outflows and feedback in the context of the overall AGN population. *Mon. Not. R. Astron. Soc.* **2014**, *441*, 3306–3347. [CrossRef]
68. Crenshaw, D.M.; Kraemer, S.B.; Schmitt, H.R.; Jaffé, Y.L.; Deo, R.P.; Collins, N.R.; Fischer, T.C. The Geometry of Mass Outflows and Fueling Flows in the Seyfert 2 Galaxy MRK 3. *Astron. J.* **2010**, *139*, 871–877. [CrossRef]
69. Woo, J.H.; Bae, H.J.; Son, D.; Karouzos, M. The Prevalence of Gas Outflows in Type 2 AGNs. *Astrophys. J.* **2016**, *817*, 108. [CrossRef]
70. Nagai, H.; Onishi, K.; Kawakatu, N.; Fujita, Y.; Kino, M.; Fukazawa, Y.; Lim, J.; Forman, W.; Vrtilek, J.; Nakanishi, K.; et al. The ALMA Discovery of the Rotating Disk and Fast Outflow of Cold Molecular Gas in NGC 1275. *Astrophys. J.* **2019**, *883*, 193. [CrossRef]
71. Kameno, S.; Sawada-Satoh, S.; Impellizzeri, C.M.V.; Espada, D.; Nakai, N.; Sugai, H.; Terashima, Y.; Kohno, K.; Lee, M.; Martín, S. A Massive Molecular Torus inside a Gas-poor Circumnuclear Disk in the Radio Galaxy NGC 1052 Discovered with ALMA. *Astrophys. J.* **2020**, *895*, 73. [CrossRef]
72. Rose, T.; Edge, A.C.; Combes, F.; Hamer, S.; McNamara, B.R.; Russell, H.; Gaspari, M.; Salomé, P.; Sarazin, C.; Tremblay, G.R.; et al. A molecular absorption line survey towards the AGN of Hydra-A. *Mon. Not. R. Astron. Soc.* **2020**, *496*, 364–380. [CrossRef]
73. Yates, J.A.; Cohen, R.J.; Hills, R.E. Submillimetre water masers in circumstellar envelopes. *Mon. Not. R. Astron. Soc.* **1995**, *273*, 529–548. [CrossRef]
74. Menten, K.M.; Melnick, G.J. 321 GHz Submillimeter Water Masers around Evolved Stars. *Astrophys. J.* **1991**, *377*, 647. [CrossRef]
75. Richards, A.M.S.; Impellizzeri, C.M.V.; Humphreys, E.M.; Vlahakis, C.; Vlemmings, W.; Baudry, A.; De Beck, E.; Decin, L.; Etoka, S.; Gray, M.D.; et al. ALMA sub-mm maser and dust distribution of VY Canis Majoris. *Astron. Astrophys.* **2014**, *572*, L9. [CrossRef]
76. Brogan, C.L.; Hunter, T.R.; Towner, A.P.M.; McGuire, B.A.; MacLeod, G.C.; Gurwell, M.A.; Cyganowski, C.J.; Brand, J.; Burns, R.A.; Caratti o Garatti, A.; et al. Sub-arcsecond (Sub)millimeter Imaging of the Massive Protocluster G358.93-0.03: Discovery of 14 New Methanol Maser Lines Associated with a Hot Core. *Astrophys. J. Lett.* **2019**, *881*, L39. [CrossRef]
77. Muller, S.; Combes, F.; Guélin, M.; Gérin, M.; Aalto, S.; Beelen, A.; Black, J.H.; Curran, S.J.; Darling, J.; V-Trung, D.; et al. An ALMA Early Science survey of molecular absorption lines toward PKS 1830-211. Analysis of the absorption profiles. *Astron. Astrophys.* **2014**, *566*, A112. [CrossRef]
78. Kuo, C.Y.; Hsiang, J.Y.; Chung, H.H.; Constantin, A.; Chang, Y.Y.; Cunha, E.d.; Pesce, D.; Chien, W.T.; Chen, B.Y.; Braatz, J.A.; et al. A More Efficient Search for H_2O Megamaser Galaxies: The Power of X-Ray and Mid-infrared Photometry. *Astrophys. J.* **2020**, *892*, 18. [CrossRef]

79. Rioja, M.J.; Dodson, R. Precise radio astrometry and new developments for the next-generation of instruments. *Astron. Astrophys. Rev.* **2020**, *28*, 6. [CrossRef]
80. Rioja, M.; Dodson, R.; Asaki, Y. Transformative Multi-Frequency Phase Transfer Solutions for ngEHT. *Galaxies* **2023**, *11*, 16.
81. Dodson, R.; Rioja, M.J.; Jung, T.H.; Sohn, B.W.; Byun, D.Y.; Cho, S.H.; Lee, S.S.; Kim, J.; Kim, K.T.; Oh, C.S.; et al. Astrometrically Registered Simultaneous Observations of the 22 GHz H_2O and 43 GHz SiO Masers toward R Leonis Minoris Using KVN and Source/Frequency Phase Referencing. *Astron. J.* **2014**, *148*, 97. [CrossRef]